coatings

MDPI

Article

Drug-Releasing Gelatin Coating Reinforced with Calcium Titanate Formed on Ti–6Al–4V Alloy Designed for Osteoporosis Bone Repair

Seiji Yamaguchi [1,*], Koji Akeda [2,*], Seine A. Shintani [1], Akihiro Sudo [2] and Tomiharu Matsushita [1]

[1] Department of Biomedical Sciences, College of Life and Health Sciences, Chubu University, 1200 Matsumoto, Kasugai 487-8501, Aichi, Japan; shintani@isc.chubu.ac.jp (S.A.S.); ma-tommy@isis.ocn.ne.jp (T.M.)
[2] Department of Orthopaedic Surgery, Mie University Graduate School of Medicine, Tsu 514-8507, Mie, Japan; a-sudou@clin.medic.mie-u.ac.jp
* Correspondence: sy-esi@isc.chubu.ac.jp (S.Y.); k_akeda@clin.medic.mie-u.ac.jp (K.A.); Tel.: +81-568-51-6420 (S.Y.); +81-59-231-5022 (K.A.)

Abstract: Ti–6Al–4V alloy has been widely used in the orthopedic and dental fields owing to its high mechanical strength and biocompatibility. However, this alloy has a poor bone-bonding capacity, and its implantation often causes loosening. Osteoporosis increases with the aging of the population, and bisphosphonate drugs such as alendronate and minodronate (MA) are used for the medical treatment. Reliable and multifunctional implants showing both bone bonding and drug releasing functions are desired. In this study, we developed a novel organic-inorganic composite layer consisting of MA-containing gelatin and calcium-deficient calcium titanate (cd–CT) with high bone-bonding and scratch resistance on Ti–6Al–4V alloy. The alloy with the composite layer formed apatite within 7 days in a simulated body fluid and exhibited high scratch resistance of an approximately 50 mN, attributable to interlocking with cd ± CT. Although the gelatin layer almost completely dissolved in phosphate-buffered saline within 6 h, its dissolution rate was significantly suppressed by a subsequent thermal crosslinking treatment. The released MA was estimated at more than 0.10 μmol/L after 7 days. It is expected that the Ti alloy with the MA-containing gelatin and cd–CT composite layer will be useful for the treatment of osteoporosis bone.

Keywords: bisphosphonate; calcium titanate; titanium alloy; apatite formation; gelatin

Citation: Yamaguchi, S.; Akeda, K.; Shintani, S.A.; Sudo, A.; Matsushita, T. Drug-Releasing Gelatin Coating Reinforced with Calcium Titanate Formed on Ti–6Al–4V Alloy Designed for Osteoporosis Bone Repair. *Coatings* **2022**, *12*, 139. https://doi.org/10.3390/coatings12020139

Academic Editor: Devis Bellucci

Received: 27 December 2021
Accepted: 21 January 2022
Published: 25 January 2022

1. Introduction

Ti–6Al–4V alloy is widely used for load bearing implants, since it is biocompatible comparatively to pure Ti metal, while it shows superior mechanical strength and corrosion resistance [1]. However, this alloy is poor in its bone bonding ability, and often results in the loosening of the implants [2,3]. This event becomes more serious in osteoporosis bone. Conferring both bone-bonding capabilities on the implant and stimulating surrounding new bone formation is a great challenge in the development of novel implants for osteoporosis bone.

In order to confer bone-bonding on Ti and its alloys, various types of inorganic coatings including a plasma spray apatite coating [4,5], titanate or titania coating by solution and heat [6,7], hydrothermal [8] and anodic oxidation [9] as well as surface roughening by blasting and acid etching [10] have been developed. Direct bone bonding of the metals was observed when coated with apatite or when apatite-formation capability, owing to the titanate or titania coatings, was conferred onto the metal surfaces [11–13]. The titanate coating showed greater adhesion than the plasma-sprayed apatite coating when the chemically graded intermediate layer with a nano-porous structure was produced by means of a solution and heat treatment [13]. Activation of preosteoblast cells was reported on the roughened surfaces with a micro-meter and nano-meter scale and their hierarchical structure [14–16]. Among the inorganic surface coatings, the calcium-deficient calcium titanate

(cd–CT) formed by the Ca-heat treatment developed by the present authors has unique surface characteristics of nano-scaled 3D network morphology, high scratch resistance, chemical durability, and abundant Ti–OH groups [17–19]. Thus, the treated metals tightly bind to both cortical and cancerous bone attributed to their high apatite formation capability [7,17–19]. We have also shown that the Ti–6Al–4V pedicle screw treated with cd–CT had a remarkably increased extraction torque compared with the untreated screw [7].

On the other hand, coatings of organic materials including biologically functional molecules composed of peptide, polysaccharide and growth factors and drugs were adhered to metal surfaces to enhance the regeneration of bone at the implant interface [20–22]. However, this type of surface modification does not permanently provide a favorable influence on osteointegration [20,21]. The metrics supporting these biomolecules and drugs are biodegradable, and the bare surface of the metal substrate is exposed after implantation for a certain period of time. Additionally, it is still challenging to achieve high adhesion between the metal substrate and polymer coatings due to large differences in surface energy between the metal and polymer. Gelatin, a biopolymer obtained from the hydrolysis of collagen, is commonly used in tissue engineering for the regeneration of skin [23], cartilage [24] and bone [25,26]. In addition to its availability and biocompatibility, gelatin offers the possibility of modulating its chemical and mechanical properties using its crosslinking capability.

Bisphosphonates (BPs), representative osteoclast inhibitors, are also shown to have a significant capacity for osteogenic induction [27–29]. BPs have been applied to bone tissue engineering technologies to develop functionalized bone tissue scaffolds with controlled release [30]. Previous studies have also shown that BP-coated titanium [31] or calcium phosphate ceramics [32] increased new bone formation around the implant and mechanical fixation. Minodronate monohydrate (MA) is one of the BPs with high potency in inhibiting bone resorption and is developed and approved for clinical use in Japan [33].

In the present study, we propose a novel coating composed of drug-releasing gelatin reinforced with the bioactive cd–CT that exhibits controlled drug release, apatite formation and high scratch resistance. The BP (minodronate) is used as a drug, and its release behavior from the coating was estimated from the degradation rate of the gelatin layer.

2. Materials and Methods

2.1. Sample Preparation

Ti–6Al–4V alloy (Ti = balance, Al = 6.18, V = 4.27 mass%, supplied by Kobelco Research Institute, Inc., Hyogo, Japan) plates with the dimensions of 10 mm × 10 mm × 1 mm were ground with a #400 diamond pad, and cleaned with acetone, 2-propanol and ultrapure water in an ultrasonic bath for 30 min each, then dried at 40 °C in an incubator overnight.

The alloy plates were subjected to NaOH–$CaCl_2$–heat–water treatment according to our previous report to form a cd–CT surface layer with high bone-bonding capability [7,17–19]. In this treatment, the samples were initially soaked in 5 mol/L NaOH (Kanto Chemical Co., Inc., Tokyo, Japan) aqueous solution at 95 °C for 24 h, and subsequently in 100 mmol/L $CaCl_2$ (Kanto Chemical Co., Inc., Tokyo, Japan) at 40 °C for 24 h with shaking in an oil bath. They were subsequently heated to 600 °C at a rate of 5 °C/min and maintained at 600 °C for 1 h, followed by natural cooling in a Fe–Cr electrical furnace. They were soaked in hot water at 80 °C for 24 h. This sequence of treatment is denoted as "Ca–heat" treatment in this study. All the reagents used in this study were of reagent grade.

After the Ca–heat treatment, the samples were dipped in 10 mL of 5–20% gelatin solution (medical grade with 316 g bloom, beMatrix LS–H, Nitta Gelatin, Osaka, Japan) pre-warmed at 60 °C in which 50 μmol/L minodronate monohydrate (minodronate; Tokyo Chemical Industry Co., Ltd., Tokyo, Japan) was dissolved in 20 mmol/L NaOH without or with the additive of 100 mmol/L $CaCl_2$ (Kanto Chemical Co., Inc., Tokyo, Japan) and/or 100 mmol/L $(NH_4)_2HPO_4$ (Kanto Chemical Co., Inc., Tokyo, Japan). The samples were pulled up at a constant speed of 1 cm/min by an electric motor, and then dried in an incubator at 40 °C overnight (This dip coating is denoted as "DC treatment").

Some of the samples with the gelatin coating were subjected to thermal cross-link (TCL) treatment [34] at 140 °C using vacuum oven (VOS-301SD, Tokyo Rikakikai Co., Ltd, Tokyo, Japan) for the desired periods from 3 to 72 h.

The treatments for each sample are summarized in Table 1.

Table 1. Notations of Ti–6Al–4V alloy samples used in this study.

Sample	Treatment		
	Ca-Heat	**Dip Coating**	**Thermal Crosslink**
Untreated	Not treated	Not treated	Not treated
CT	Treated	Not treated	Not treated
CT(X)G	Treated	X% gelatin (X = 5–20)	Not treated
CT(X)G + MA	Treated	X% gelatin + 50 μmol/L minodronate	Not treated
CT(X)G + MA + Ca and/or P	Treated	X% gelatin + 50 μmol/L minodronate + 100 mmol/L $CaCl_2$ and/or 100 mmol/L $(NH_4)_2HPO_4$	Not treated
CT(X)G + MA + Ca and/or P + (Y)TCL	Treated	X% gelatin + 50 μmol/L minodronate + 100 mmol/L $CaCl_2$ and/or 100 mmol/L $(NH_4)_2HPO_4$	Y hours at 140 °C in vacuum (Y = 6–144)

2.2. Viscosity of Gelatin Solution

The viscosity of the gelatin solution (5–20%) with or without additives as a function of gelatin concentration was measured by Brookfield viscometer (LVDVNextCP; Brookfield Engineering Laboratories, Inc., Middleboro, MA, USA) according to JIS8803 (Japanese Industrial Standards Z8803:2011, Methods for viscosity measurement of liquid). The spindle speeds (and corresponding shear rates) were optimized for each sample between 11.52 and 576 1/s (shear rates were 3 to 150 rpm), and four different spindle speeds were examined for each sample instead of increasing the number of replicates. The measurements were performed using 2 mL samples at 60 °C, and the viscosity (mPa·s) of the sample obtained for each run after a 30 s holding time was used for analysis.

2.3. Surface Characteristics

2.3.1. Scanning Electron Microscopy and Energy Dispersive X-ray Analysis

The surface and cross-sectional area of the prepared samples were coated with a Pt/Pd thin film and observed under a field-emission scanning electron microscope (FE-SEM, S-4300, Hitachi Co., Tokyo, Japan) equipped with energy dispersive X-ray analysis (EDX, EMAX-7000, Horiba Ltd., Kyoto, Japan) at an accelerated voltage of 15 kV and an electric current of 9–11 μA. In EDX analysis, C, O, Ti, Al, V, Ca, P, Na and Cl of the sample surfaces were examined using an accelerated voltage of 9 kV with a electric current of 10 μA. Five locations were measured, and their averaged values (a.v.) and standard deviations (s.d.) were used (described as a.v. ± s.d.).

2.3.2. Thin-Film X-ray Diffraction

Surface crystalline structures of the samples were analyzed using TF-XRD (Model RNT-2500, Rigaku Co., Akishima, Tokyo, Japan), employing a CuKα X–ray source operating at 50 kV and 200 mA. The glancing angle of the incident beam was set to an angle of 1° against the sample surface.

2.3.3. Scratch Resistance Measurements

The scratch resistance of the surface layer formed on the Ca–heat-treated samples with or without gelatin layer was measured using a thin film scratch tester (Model CSR-2000, Rhesca Co., Hino, Tokyo, Japan). A stylus with a diameter of 5 μm with a spring constant of 200 g/mm was employed and pressed onto the samples with a loading rate of 100 mN/min, an amplitude of 100 μm and a scratch speed of 10 μm/s, based on the data in the JIS R-3255 standard (Japanese Industrial Standard R-3255, Test methods for adhesion of thin films on

glass substrate). Five areas were measured for each sample, and their averaged values and standard deviations were used.

2.3.4. Dissolution of Gelatin

The samples with the gelatin layer with $CaCl_2$ and MA additives subjected to TCL treatment were immersed in 2 mL of phosphate buffered saline (PBS) and gently shaken at a speed of 50 strokes/min at 36.5 °C. The Ca^{2+} ion concentrations released in PBS as a result of gelatin dissolution (the solvent/sample ratio was 2 mL/2.4 cm^2) were measured by inductively coupled plasma emission spectroscopy (ICP, SPS3100, Seiko Instruments Inc., Chiba, Japan) after the determined periods of soaking up to 7 days. The PBS solution was refreshed at each determined period, and the measurement was repeated 3 times for independently prepared samples. Their averaged values and standard deviations were calculated. The released MA concentration was estimated from the Ca^{2+} ion concentrations under the assumption of homogeneous Ca^{2+} ion distribution in a gelatin layer.

2.4. Apatite Formation

The samples with the gelatin layer with or without additives of $CaCl_2$ and/or $(NH_4)_2HPO_4$ were immersed in 24 mL of a pre-warmed simulated body fluid (SBF, 36.5 °C) with ion concentrations nearly equal to those of human blood plasma for 7 days at 36.5 °C [35]. After removal from the SBF, apatite formation on the sample surface was observed by FE-SEM and TF-XRD.

2.5. Statistical Analysis

Statistical tests were performed with a library of statistical software tools (R language; version 3.6.1, The R Foundation, Vienna, Austria). The normality of the scratch resistance measurement results was tested by the Shapiro–Wilk test. As a result, normality was not rejected for all data. The comparison between the control group and the other groups was tested by the multi-group test (Dunnett's test). The significance level for all statistical analyses was $p < 0.05$.

3. Results

3.1. Viscosity of Gelatin

The viscosity of the 5% gelatin solution was 3.5 mPa·s, and this increased to 15.1 and 184.2 mPa·s with increasing gelatin concentration to 10 and 20%, respectively, as shown in Figure 1. The addition of 100 mmol/L $CaCl_2$ and 50 µmol/L MA into 10% gelatin slightly increased the viscosity to 16.6 mPa·s.

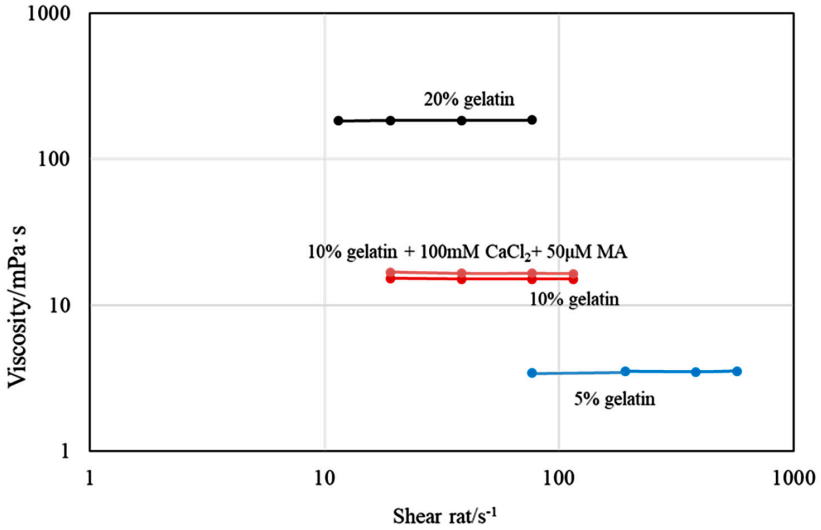

Figure 1. The viscosity of the gelatin solution as a function of gelatin concentration.

3.2. The Surface Characteristics

Figure 2 shows the surface and cross-sectional SEM images of Ti–6Al–4V samples subjected to Ca–heat, and subsequent DC treatment without and with the additives. After the Ca–heat treatment, a nano-structured three-dimensional network surface layer with 1.7 μm thickness was produced on the alloy substrate. This layer was composed of cd–CT, rutile and anatase as reported in our previous study [17].

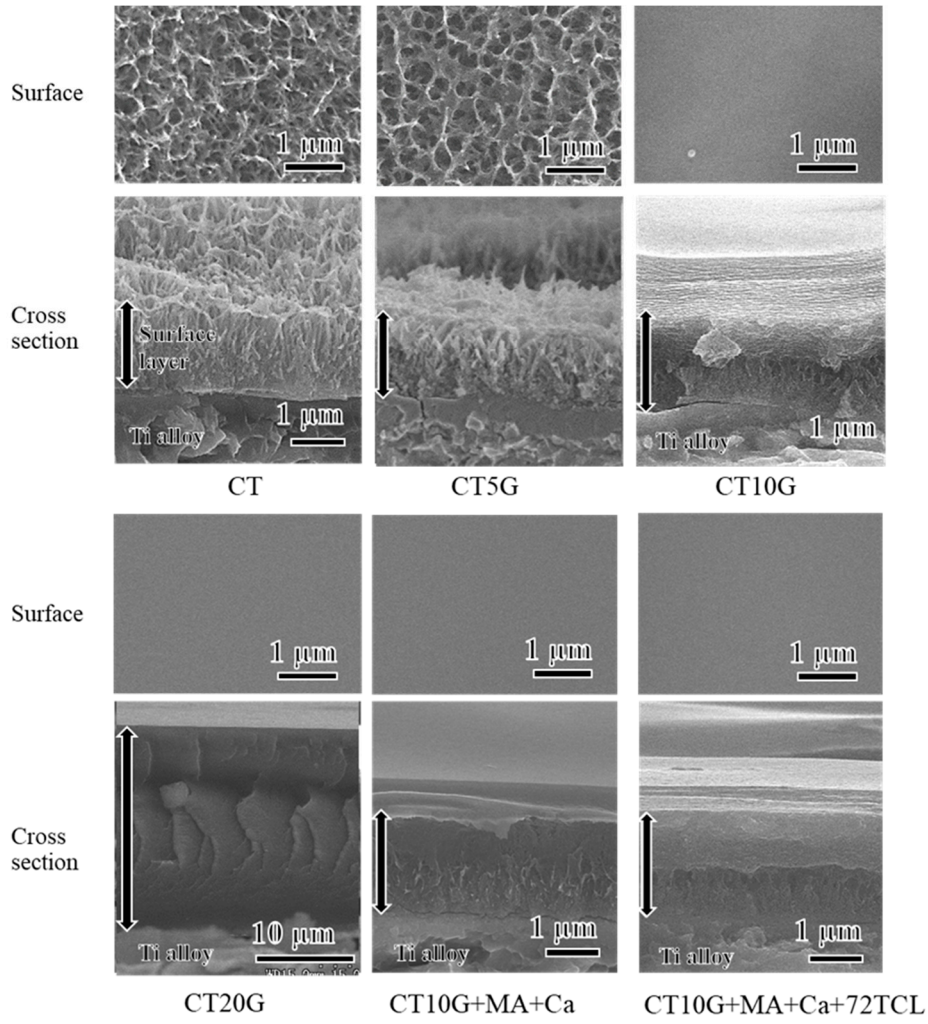

Figure 2. Surface and cross-sectional SEM images of Ca-heat treated Ti–6Al–4V alloy subjected to dip coating with various additives and subsequent thermal cross-link treatment.

When the treated sample was dipped in 5% gelatin solution, only slight modification with the gelatin was observed. In contrast, the surface morphology became smooth due to the complete surface coverage by the gelatin when the metal sample was dipped in 10% gelatin (see CT10G). Cross-sectional observation of CT10G revealed that the gelatin permeated through the nano-structured network to form an inorganic–organic composite layer approximately 2 μm in thickness. The thickness of the gelatin layer increased to about 25 μm by increasing the gelatin concentration to 20%, accompanied by a deposition of a single and thick gelatin layer on the inorganic–organic composite. The additives of 100 mmol/L $CaCl_2$ and 50 μmol/L MA did not apparently affect the thickness of the 10% gelatin coating. The surface and cross-sectional morphologies were maintained even after the TCL treatment.

Table 2 shows the chemical composition of the sample surfaces. The amounts of 2.9% Ca and 23.9% Ti were detected on the sample CT, and these values decreased with the DC treatment using 5–20% gelatin solution: the higher the gelatin concentrations, the

lower the Ca and Ti amounts. In contrast, the amount of carbon increased with increasing gelatin concentration. These results are consistent with the SEM results, in which a thicker gelation layer was observed on the DC sample using higher concentration of gelatin. Some amounts of Ca and/or P attributed to the additives were detected on the DC samples when the $CaCl_2$ and/or $(NH_4)_2HPO_4$ were added in the gelatin solution (see the samples of "CT10G + MA + Ca", "CT10G + MA + P" and "CT10G + MA + Ca and P"). The surface chemical composition of CT10G + MA + Ca was maintained even after TCL treatment for 72 h.

Table 2. EDX results on the Ti–6Al–4V alloy surfaces treated with Ca–heat followed by gelatin coating and thermal crosslinking.

Sample	Element/at.%								
	C	O	Ti	Al	V	Ca	P	Na	Cl
Untreated	5.4 ± 1.2	0.0 ± 0.0	80.9 ± 0.9	9.4 ± 0.1	4.3 ± 0.2	0.0 ± 0.0	0.0 ± 0.0	0.0 ± 0.0	0.0 ± 0.0
CT	7.4 ± 0.5	64.4 ± 0.4	23.9 ± 2.9	0.6 ± 0.1	0.8 ± 0.1	2.9 ± 0.2	0.0 ± 0.0	0.0 ± 0.0	0.0 ± 0.0
CT5G	27.9 ± 1.7	53.5 ± 0.9	15.7 ± 0.6	0.4 ± 0.0	0.4 ± 0.1	2.0 ± 0.1	0.0 ± 0.0	0.2 ± 0.0	0.0 ± 0.0
CT10G	61.3 ± 2.9	35.4 ± 1.6	2.3 ± 1.1	0.0 ± 0.0	0.1 ± 0.0	0.5 ± 0.2	0.0 ± 0.0	0.3 ± 0.0	0.2 ± 0.0
CT20G	63.9 ± 1.0	35.6 ± 1.1	0.0 ± 0.0	0.0 ± 0.0	0.0 ± 0.0	0.0 ± 0.0	0.0 ± 0.0	0.3 ± 0.1	0.1 ± 0.0
CT10G + MA + Ca	64.6 ± 0.3	32.1 ± 0.4	0.1 ± 0.0	0.0 ± 0.0	0.0 ± 0.0	0.8 ± 0.1	0.0 ± 0.0	0.3 ± 0.0	2.0 ± 0.1
CT10G + MA + P	66.7 ± 0.2	32.3 ± 0.3	0.2 ± 0.1	0.0 ± 0.0	0.0 ± 0.0	0.0 ± 0.0	0.4 ± 0.0	0.1 ± 0.0	0.2 ± 0.0
CT10G + MA + Ca and P	63.1 ± 3.8	32.6 ± 1.7	0.4 ± 0.8	0.0 ± 0.0	0.0 ± 0.0	0.4 ± 0.6	0.4 ± 0.5	0.4 ± 0.1	2.5 ± 0.6
CT10G + MA + Ca + 72TCL	65.4 ± 0.1	30.8 ± 0.2	0.2 ± 0.0	0.0 ± 0.0	0.0 ± 0.0	1.0 ± 0.0	0.0 ± 0.0	0.3 ± 0.0	2.4 ± 0.1

The TF-XRD profiles in Figure 3 show that the peaks of cd–CT and rutile were detected on the sample CT, and these remained after DC treatment using 5% gelatin solution. In contrast, their intensities decreased with increasing gelatin concentration due to the development of the gelatin layer. Although the sole addition of $CaCl_2$ or $(NH_4)_2HPO_4$ into the MA-containing gelatin solution did not apparently change the profiles of CT10G, the addition of both $CaCl_2$ and $(NH_4)_2HPO_4$ generated large peaks attributed to brushite, indicating precipitation of brushite particles in the gelatin solution. The profile of the sample CT10G + MA + Ca was not apparently changed even after the TCL treatment for 72 h.

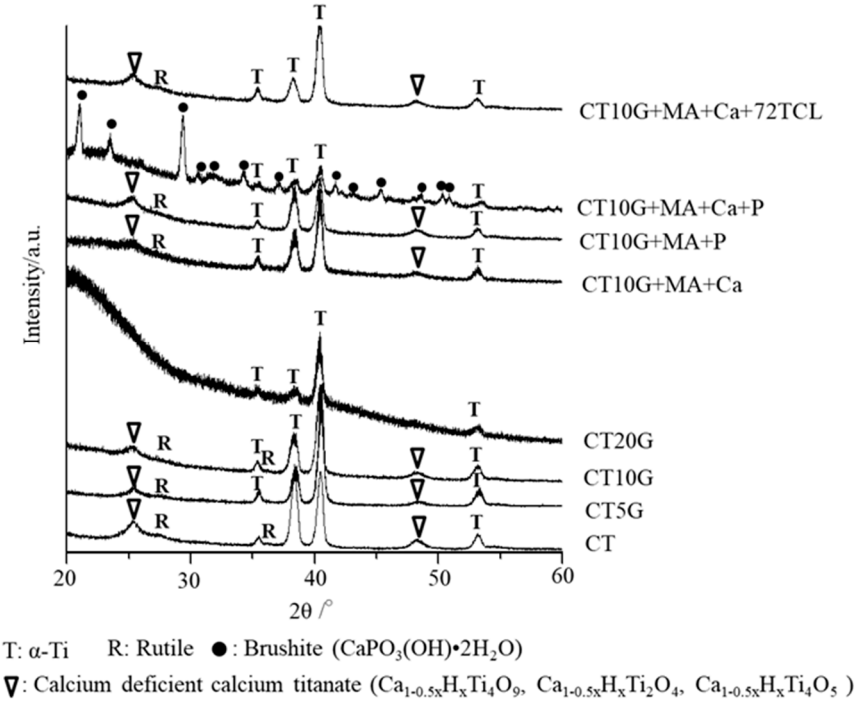

Figure 3. XRD profiles of Ca–heat-treated Ti–6Al–4V alloy subjected to dip coating with various additives and subsequent thermal cross–link treatment.

Critical scratch loads of the samples measured by scratch tester are summarized in Table 3. The critical scratch load was 42.6 mN for the CT sample, and this value increased to 47.2 and 54.0 mN for the CT5G and CT10G samples, respectively. Statistically significant differences were observed between CT and CT10G ($p < 0.001$). Similar values were observed on the 10% DC-treated samples with the additives and subsequent TCL treatment, in which statistically significant differences ($p < 0.001$) were detected on all the samples except CT10G + MA + Ca ($p = 0.092$). For the comparison, the critical scratch load on the 10% DC-treated alloy without cd–CT layer was measured, which was as low as 4.1 mN ($p < 0.001$).

Table 3. Critical scratch loads of the Ti–6Al–4V treated with Ca–heat followed by gelatin coating and thermal crosslinking.

Sample.	Critical Scratch Load/mN	Statistically Significant Difference
CT	42.6 ± 3.3	-
CT5G	47.2 ± 6.6	($p = 0.3428$)
CT10G	54.0 ± 4.6	† ($p < 0.001$)
CT10G + MA + Ca	49.0 ± 2.5	($p = 0.092$)
CT10G + MA + P	59.4 ± 4.4	† ($p < 0.001$)
CT10G + MA + Ca + P	54.6 ± 4.0	† ($p < 0.001$)
CT10G + MA + Ca + 72TCL	55.0 ± 3.7	† ($p < 0.001$)
10G *	4.1 ± 0.3	† ($p < 0.001$)

* 10% gelatin was dip-coated without Ca-heat treatment. † Statistical significant difference toward CT ($p < 0.05$).

3.3. Apatite Formation

Figure 4 shows the SEM images of the treated samples after being soaked in SBF for 7 days. Apatite particles fully deposited on the CT and CT5G samples, while they partially deposited on the CT10G and CT20G samples. When the $CaCl_2$ or $(NH_4)_2HPO_4$ was solely added into the 10% gelatin solution, apatite formation increased to be fully deposited on the sample surfaces (CT10G + MA + Ca, CT10G + MA + P). In contrast, scarce and inhomogeneous apatite formation was observed when both $CaCl_2$ and $(NH_4)_2HPO_4$ were added into the gelatin solution (CT10G + MA + Ca and P).

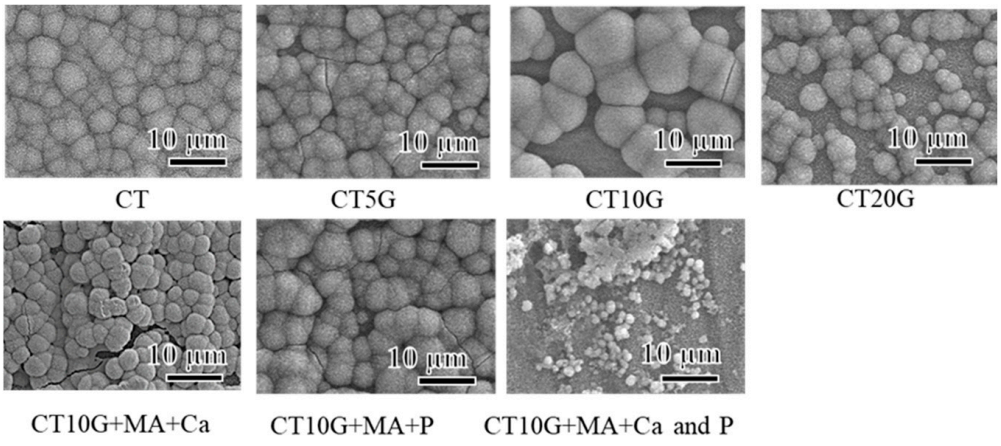

Figure 4. SEM images of surfaces of Ca–heat-treated Ti–6Al–4V alloy soaked in SBF for 7 days following dip coat treatment with various additives.

Figure 5 shows XRD profiles of these samples. The peaks at around 26 and 32 degrees in 2θ that are attributed to hydroxyapatite were observed on all the samples, while CT10G + MA + Ca + P showed the smallest peak intensity.

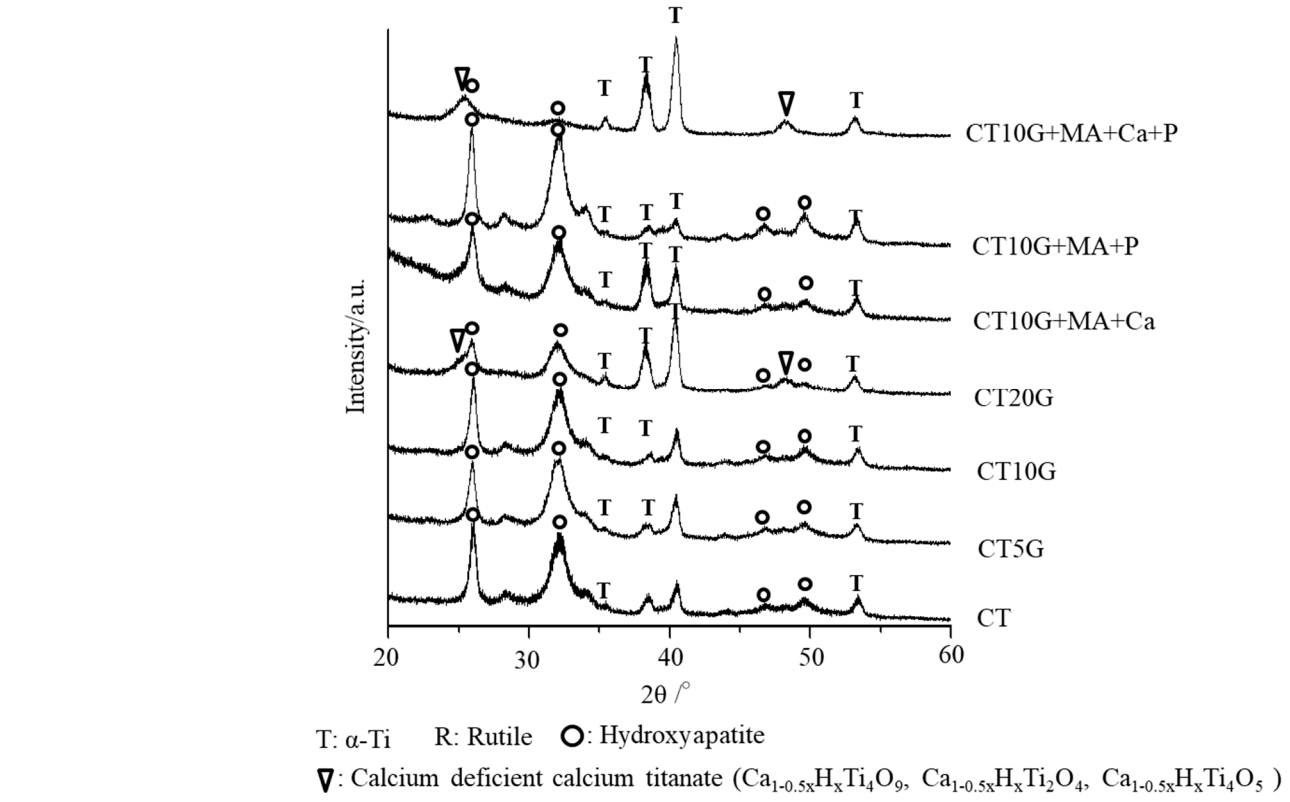

Figure 5. XRD profiles of surfaces of Ca–heat-treated Ti–6Al–4V alloy soaked in SBF for 7 days following dip coat treatment with various additives.

When the 10%-DC samples with the additives of Ca or P were subjected to TCL treatment, the former maintained its apatite formation even after 72 h of TCL treatment (Figure 6). On the contrary, the latter lost its apatite formation within 3 h of TCL treatment.

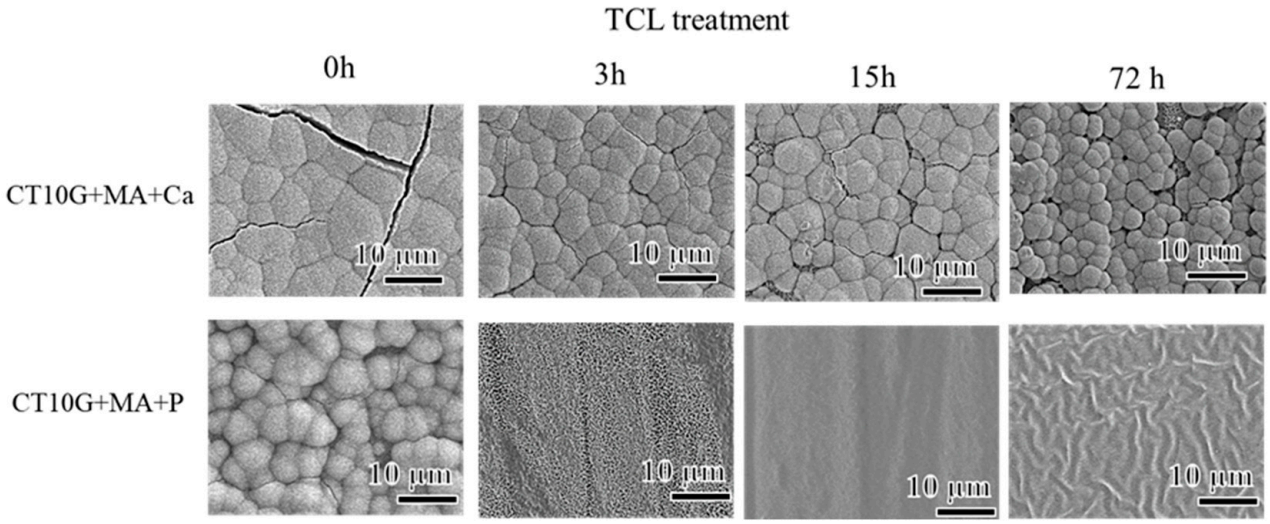

Figure 6. SEM images of surfaces of Ca–heat-treated Ti–6Al–4V alloy soaked in SBF for 7 days following dip coat and subsequent thermal cross-link treatment.

3.4. Gelatin Dissolution

Gelatin dissolution of the sample CT10G + MA + Ca with or without TCL treatment for the periods of 3–72 h was examined by measuring the Ca amount in PBS after the determined soaking period. The released MA concentration was calculated from the disso-

lution rate under the assumption that Ca is homogeneously distributed in gelatin. It can be seen in Figure 7 that Ca ions were rapidly released within 6 h and reached a stable value after 6 h for CT10G + MA + Ca, suggesting that the gelatin almost completely dissolved within 6 h. The initial gelatin dissolution rate decreased with increasing the periods of TCL treatment up to 72 h, indicating that the TCL treatment effectively suppressed gelatin dissolution. The total amount of MA released into PBS after 7 days was calculated to be 0.13 and 0.10 μmol/L for CT10G + MA + Ca and CT10G + MA + Ca + 72TCL, respectively. When the sample surfaces after being soaked in PBS for 7 days were observed under SEM, it was found that some amount of gelatin remained on the sample treated with TCL for 72 h, while almost complete dissolution of gelatin was observed on other samples (Figure 8). The cd–CT layer with nano-scaled network morphology remained even after the dissolution of gelatin for all of the samples.

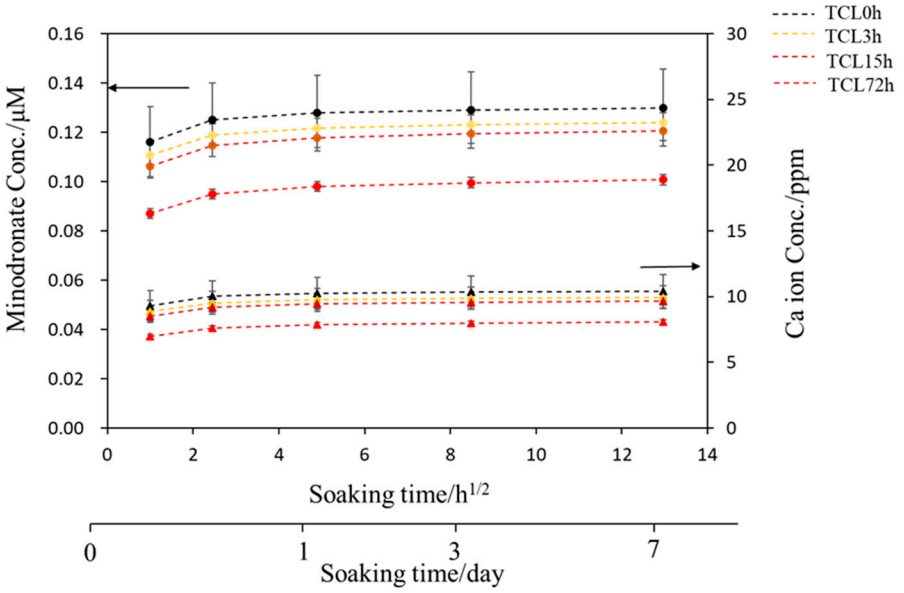

Figure 7. Calcium ion release into PBS from the sample CT10G + MA + Ca without or with thermal cross-link treatment for periods of 3–72 h. The released minodonate was estimated from the Ca ion concentration in PBS for each soaking period.

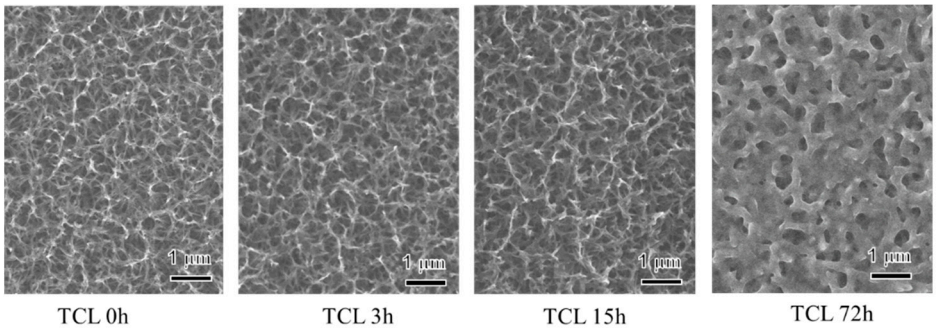

Figure 8. SEM images of the surfaces of the sample CT10G + MA + Ca without or with thermal cross-link treatment for periods of 3–72 h that were soaked in PBS for 7 days.

4. Discussion

A three-dimensional network structure composed of the bioactive cd–CT was initially produced on Ti–6Al–4V alloy by the Ca–heat treatment. It was shown that the cd–CT layer is hydrophilic and has superior scratch resistance, chemical durability, abundant Ti–OH groups, and reliable apatite-formation capability for inducing bone-bonding [7,17–19]. The remarkable bone-bonding capacity of the cd–CT was reported in our previous reports, in which Ti and Ti–Zr–Nb–Ta system alloys such as Ti-15Zr–4Nb–4Ta exhibited significantly

higher critical detaching failure load and bone contact area than untreated Ti even in an early period of 4 weeks after implantation [19]. When the cd–CT was formed on the Ti–6Al–4V pedicle screw by the Ca–heat treatment, it exhibited higher extraction torque compared with the untreated screw [7]. It was also demonstrated that many bone fragments remained on the treated metals in both cases [18], indicating that fracture occurred not at the bone–implant interface but in the bone itself. Nevertheless, osteoinductivity and osteogenesis, in addition to osteoconductivity, are also desired in order to achieve further reliable bone regeneration, which are usually induced by functional organic materials such as cytokines, proteins and drugs [36]. In this study, the bioactive cd–CT layer was dipped into the medical-grade gelatin solution including MA to form an inorganic–organic composite releasing a bisphosphonate drug for the treatment of osteoporosis bone.

Generally, it is challenging to achieve high adhesion between the metal substrate and polymer coatings due to large differences in surface energy between the metal and polymer [37]. In the present study, the gelatin easily penetrated into the 3D network structure due to the hydrophilic nature of the cd–CT. Its coating thickness increased with the increase in gelatin concentration as a result of the increased viscosity of the gelatin solution (Figure 1). When the 10% gelatin was used, the thickness of the gelatin coating became comparative to that of the cd–CT layer (Figure 2), which seems to be suitable for practical use. Therefore, we determined the 10% gelatin, and thus the corresponding viscosity of 15.1 mPa·s, as an optimized condition. It was also confirmed that the thickness of the coated gelatin as well as the viscosity of the gelatin solution was almost not affected by the additives such as MA, $CaCl_2$ and $(NH_4)_2HPO_4$ (Figures 1 and 2). Thus, the produced inorganic–organic composite layer exhibits a high scratch resistance of about 50 mN owing to an interlocking effect between the 3D network frames of cd–CT and gelatin matrix.

When the gelatin-coated alloy with the cd–CT layer was soaked in SBF, its apatite formation decreased with an increasing gelatin concentration (Figure 4). Since the apatite formation on the Ti and its alloys with cd–CT was attributed to the release of Ca^{2+} ions from the cd–CT and abundant Ti–OH groups [17,38,39], the decrease in apatite formation on the gelatin-coated alloys was probably due to the suppression of Ca^{2+} ion release and the hiding of Ti–OH groups by the coated gelatin. When the $CaCl_2$ or $(NH_4)_2HPO_4$ as well as MA were solely added to the gelatin, the coated alloys formed apatite fully on their surfaces. The increased apatite formation might be due to the Ca^{2+} or HPO_4^{2-} ions that were released from the dissolved gelatin in SBF. Interestingly, scarce and inhomogeneous precipitation of apatite was observed on the DC-treated alloy with the additives of both $CaCl_2$ and $(NH_4)_2HPO_4$. This may be caused by rapid calcium phosphate precipitation in the gelation solution before the soaking in SBF. Indeed, brushite peaks were detected on the sample surface by XRD (Figure 3). It is seen in Figure 6 that the additives of $CaCl_2$ were also effective in inducing apatite formation even for the TCL-treated alloys while $(NH_4)_2HPO_4$ was not. This might be because the rate of gelatin dissolution was suppressed by the TCL treatment, suggesting that calcium ions are more effective for apatite formation than phosphate ions by effectively increasing the ionic activity product of apatite, $Ca_{10}(PO)_4(OH)_2$, than phosphate ions.

When the gelatin-coated alloy without TCL treatment was soaked in PBS, its gelatin layer rapidly dissolved within 6 h. It has been reported that thermal and chemical crosslinking can enhance the physical durability of gelatin [34,40]. In the present study, the thermal crosslinking method developed by Tsujimoto et al. was adopted to achieve slow dissolution of gelatin. It can be seen in Figure 7 that the dissolution rate was significantly suppressed by TCL treatment for 72 h. The estimated amount of MA released into PBS during the 7 days from the treated alloy was 0.10 μmol/L, which is effective for suppressing the activity of osteoclast cells [41]. Although the gelatin dissolved in a relatively short period of time in the aqueous solution, the cd–CT layer is chemically stable, as shown in Figure 8. It is expected that the treated layer with the composite of MA-containing gelatin and the cd–CT layer slowly releases MA to improve the bone mass of surrounding tissue and bonds to bone because of its apatite formation. Thus, the obtained bone-bonding is expected to

be stable even after the dissolution of the gelatin layer, since the cd–CT layer is stable even under a simulated body environment. Further in vivo studies using animal model of osteoporosis are needed to prove the usefulness of the developed material for therapeutic treatment for osteoporosis bone.

5. Conclusions

The novel composite layer of minodronate-containing gelatin and calcium-deficient calcium titanate was produced on Ti–6Al–4V alloy. The treated alloy exhibited high scratch resistance, apatite formation capacity and slow release of minodronate, effective for medical treatment in osteoporosis bone, and thus should be useful for orthopedic implants.

Author Contributions: Conceptualization, S.Y. and K.A. methodology, S.Y.; software, S.A.S.; validation, K.A., A.S., and T.M.; formal analysis, S.Y.; investigation, S.Y.; resources, S.Y.; data curation, K.A., S.A.S., and A.S. and T.M.; writing—original draft preparation, S.Y. and K.A.; writing—review and editing, T.M. and S.A.S.; visualization, S.Y.; supervision, A.S. and T.M.; project administration, S.Y.; funding acquisition, K.A. All authors have read and agreed to the published version of the manuscript.

Funding: This study was supported by Grant-in-Aid for Scientific Research (KAKENHI) (C) (Grant Number 15K10402) and Japan Agency for Medical Research and Development (AMED) seeds A (Grant Number: A78).

Institutional Review Board Statement: Not applicable.

Informed Consent Statement: Not applicable.

Data Availability Statement: The data presented in this study are available on request from the corresponding author.

Conflicts of Interest: The authors declare no conflict of interest and the funders had no role in the design of the study; in the collection, analyses, or interpretation of data; in the writing of the manuscript, or in the decision to publish the results.

References

1. Hanawa, T. Overview of metals and applications. In *Metals for Biomedical Devices*; Niinomi, M., Ed.; Woodhead Publishing: Cambridge, UK, 2019; pp. 3–30.
2. Wu, J.C.; Huang, W.C.; Tsai, H.W.; Ko, C.C.; Wu, C.L.; Tu, T.H.; Cheng, H. Pedicle screw loosening in dynamic stabilization: Incidence, risk, and outcome in 126 patients. *Neurosurg. Focus* **2011**, *31*, E9. [CrossRef] [PubMed]
3. Tokuhashi, Y.; Matsuzaki, H.; Oda, H.; Uei, H. Clinical course and significance of the clear zone around the pedicle screws in the lumbar degenerative disease. *Spine* **2008**, *33*, 903–908. [CrossRef] [PubMed]
4. Wang, H.; Eliaz, N.; Xiang, Z.; Hsu, H.-P.; Spector, M.; Hobbs, L.W. Early bone apposition in vivo on plasma-sprayed and electrochemically deposited hydroxyapatite coatings on titanium alloy. *Biomaterials* **2006**, *23*, 4192–4203. [CrossRef] [PubMed]
5. Su, Y.; Cockerill, I.; Zheng, Y.; Tang, L.; Qin, Y.-X.; Zhu, D. Biofunctionalization of metallic implants by calcium phosphate coatings. *Bioact. Mater.* **2019**, *4*, 196–206. [CrossRef] [PubMed]
6. Kokubo, T.; Yamaguchi, S. Simulated body fluid and the novel bioactive materials derived from it. *J. Biomed. Mater. Res. Part A* **2019**, *107*, 968–977. [CrossRef]
7. Akeda, K.; Yamaguchi, S.; Matsushita, T.; Kokubo, T.; Murata, K.; Takegami, N.; Matsumine, A.; Sudo, A. Bioactive pedicle screws prepared by chemical and heat treatments improved biocompatibility and bone-bonding ability in canine lumbar spines. *PLoS ONE* **2018**, *13*, e196766. [CrossRef]
8. Park, J.-W.; Park, K.-B.; Suh, J.-Y. Effects of calcium ion incorporation on bone healing of Ti6Al4V alloy implants in rabbit tibiae. *Biomaterials* **2007**, *28*, 3306–3313. [CrossRef] [PubMed]
9. Huang, Y.; Wang, W.; Zhang, X.; Liu, X.; Xu, Z.; Han, S.; Su, Z.; Liu, H.; Gao, Y.; Yang, H. A prospective material for orthopedic applications: Ti substrates coated with a composite coating of titania-nanotubes layer and a silver-manganese-doped hydroxyapatite layer. *Ceram. Int.* **2018**, *44*, 5528–5542. [CrossRef]
10. Yang, G.L.; He, F.M.; Yang, X.F.; Wang, X.X.; Zhao, S.F. Bone responses to titanium implants surface-roughened by sandblasted and double etched treatments in a rabbit model. *Oral Surg. Oral Med. Oral Pathol. Oral Radiol. Endod.* **2008**, *106*, 516–524. [CrossRef]
11. Harun, W.S.W.; Harun, W.S.W.; Alias, J.; Zulkifli, F.H.; Kadirgama, K.; Ghani, S.A.C.; Shariffuddin, J.H.M. A comprehensive review of hydroxyapatite-based coatings adhesion on metallic biomaterials. *Ceram. Int.* **2018**, *44*, 1250–1268. [CrossRef]

12. Spriano, S.; Yamaguchi, S.; Baino, F.; Ferraris, S. A critical review of multifunctional titanium surfaces: New frontiers or improving osseointegration and host response, avoiding bacteria contamination. *Acta Biomater.* **2018**, *79*, 1–22. [CrossRef] [PubMed]
13. Kawai, T.; Takemoto, M.; Fujibayashi, S.; Tanaka, M.; Akiyama, H.; Nakamura, T.; Matsuda, S. Comparison between alkali heat treatment and sprayed hydroxyapatite coating on thermally-sprayed rough Ti surface in rabbit model: Effects on bone-bonding ability and osteoconductivity. *J. Biomed. Mater. Res. B Appl. Biomater.* **2015**, *103*, 1069–1081. [CrossRef] [PubMed]
14. Zhang, Z.; Xu, R.; Yang, Y.; Liang, C.; Yu, X.; Liu, Y.; Wang, T.; Yu, Y.; Deng, F. Micro/nano-textured hierarchical titanium topography promotes exosome biogenesis and secretion to improve osseointegration. *J. Nanobiotechnol.* **2021**, *19*, 78. [CrossRef] [PubMed]
15. Le, P.T.M.; Shintani, S.A.; Takadama, H.; Ito, M.; Kakutani, T.; Kitagaki, H.; Terauchi, S.; Ueno, T.; Nakano, H.; Nakajima, Y.; et al. Bioactivation Treatment with Mixed Acid and Heat on Titanium Implants Fabricated by Selective Laser Melting Enhances Preosteoblast Cell Differentiation. *Nanomaterials* **2021**, *11*, 987. [CrossRef] [PubMed]
16. Isaac, J.; Galtayries, A.; Kizuki, T.; Kokubo, T.; Berdal, A.; Sautier, J.M. Bioengineered titanium surfaces affect the gene-expression and phenotypic response of osteoprogenitor cells derived from mouse calvarial bones. *ECM* **2010**, *20*, 178–196. [CrossRef] [PubMed]
17. Yamaguchi, S.; Takadama, H.; Matsushita, T.; Nakamura, T.; Kokubo, T. Apatite-forming ability of Ti-15Zr-4Nb-4Ta alloy induced by calcium solution treatment. *J. Mater. Sci. Mater. Med.* **2010**, *21*, 439–444. [CrossRef]
18. Tanaka, M.; Takemoto, M.; Fujibayashi, S.; Kawai, T.; Yamaguchi, S.; Kizuki, T.; Matsushita, T.; Kokubo, T.; Nakamura, T.; Matsuda, S. Bone bonding ability of a chemically and thermally treated low elastic modulus Ti alloy: Gum metal. *J. Mater. Sci. Mater. Med.* **2014**, *25*, 635–643. [CrossRef]
19. Fukuda, A.; Takemoto, M.; Saito, T.; Fujibayashi, S.; Neo, M.; Yamaguchi, S.; Kizuki, T.; Matsushita, T.; Niinomi, M.; Kokubo, T.; et al. Bone bonding bioactivity of Ti metal and Ti–Zr–Nb–Ta alloys with Ca ions incorporated on their surfaces by simple chemical and heat treatments. *Acta Biomater.* **2011**, *7*, 1379–1386. [CrossRef]
20. Al-Zubaidi, S.M.; Madfa, A.A.; Mufadhal, A.A.; Aldawla, M.A.; Hameed, O.S.; Yue, X.-G. Improvements in clinical durability from functional biomimetic metallic dental implants. *Front. Mater.* **2020**, *7*, 106. [CrossRef]
21. Meng, H.W.; Chien, E.Y.; Chien, H.H. Dental implant bioactive surface modifications and their effects on osseointegration: A review. *Biomark. Res.* **2016**, *4*, 24. [CrossRef]
22. Torres, Y.; Begines, B.; Beltr'an, A.M.; Boccaccini, A.R. Deposition of bioactive gelatin coatings on porous titanium: Influence of processing parameters, size and pore morphology. *Surf. Coat. Technol.* **2021**, *421*, 127366. [CrossRef]
23. Smandri, A.; Nordin, A.; Hwei, N.M.; Chin, K.Y.; Abd Aziz, I.; Fauzi, M.B. Natural 3Dprinted bioinks for skin regeneration and wound healing: A systematic review. *Polymers* **2020**, *12*, 1782. [CrossRef] [PubMed]
24. Ngadimin, K.; Stokes, A.; Gentile, P.; Ferreira-Duarte, A.M. Biomimetic hydrogels designed for cartilage tissue engineering. *Biomater. Sci.* **2021**, *9*, 4246–4259. [CrossRef] [PubMed]
25. Dong, Z.; Yuan, Q.; Huang, K.; Xu, W.; Liu, G.; Gu, Z. Gelatin methacryloyl (GelMA)-based biomaterials for bone regeneration. *RSC Adv.* **2019**, *9*, 17737–17744. [CrossRef]
26. Ranganathan, S.; Balagangadharan, K.; Selvamurugan, N. Chitosan and gelatinbasedelectrospun fibers for bone tissue engineering. *Int. J. Biol. Macromol.* **2019**, *133*, 354–364. [CrossRef] [PubMed]
27. Fleisch, H. Bisphosphonates: Mechanisms of action. *Endocr. Rev.* **1998**, *19*, 80–100. [CrossRef]
28. Garcia-Moreno, C.; Serrano, S.; Nacher, M.; Farre, M.; Diez, A.; Marinoso, M.L.; Carbonell, J.; Mellibovsky, L.; Nogués, X.; Ballester, J.; et al. Effect of alendronate on cultured normal human osteoblasts. *Bone* **1998**, *22*, 233–239. [CrossRef]
29. Wang, C.Z.; Chen, S.M.; Chen, C.H.; Wang, C.K.; Wang, G.J.; Chang, J.K.; Ho, M.L. The effect of the local delivery of alendronate on human adipose-derived stem cell-based bone regeneration. *Biomaterials* **2010**, *31*, 8674–8683. [CrossRef]
30. Cui, Y.; Zhu, T.; Li, D.; Li, Z.; Leng, Y.; Ji, X.; Liu, H.; Wu, W.; Ding, J. Bisphosphonate-Functionalized Scaffolds for Enhanced Bone Regeneration. *Adv. Healthc. Mater.* **2019**, *8*, e1901073. [CrossRef]
31. Kajiwara, H.; Yamaza, T.; Yoshinari, M.; Goto, T.; Iyama, S.; Atsuta, I.; Kido, M.A.; Tanaka, T. The bisphosphonate pamidronate on the surface of titanium stimulates bone formation around tibial implants in rats. *Biomaterials* **2005**, *26*, 581–587. [CrossRef]
32. Peter, B.; Gauthier, O.; Laib, S.; Bujoli, B.; Guicheux, J.; Janvier, P.; van Lenthe, G.H.; Müller, R.; Zambelli, P.-Y.; Bouler, J.-M.; et al. Local delivery of bisphosphonate from coated orthopedic implants increases implants mechanical stability in osteoporotic rats. *J. Biomed. Mater. Res. Part A* **2006**, *76*, 133–143. [CrossRef]
33. Matsumoto, T.; Endo, I. Minodronate. *Bone* **2020**, *137*, 115432. [CrossRef] [PubMed]
34. Tsujimoto, H.; Tanzawa, A.; Miyamoto, H.; Horii, T.; Tsuji, M.; Kawasumi, A.; Tamura, A.; Wang, Z.; Abe, R.; Tanaka, S.; et al. Biological properties of a thermally crosslinked gelatin film as a novel anti-adhesive material: Relationship between the biological properties and the extent of thermal crosslinking. *J. Biomater. Mater. Res. Part B Appl. Biomater.* **2015**, *103*, 1511–1518. [CrossRef]
35. Kokubo, T.; Takadama, H. How useful is SBF in predicting in vivo bone bioactivity? *Biomaterials* **2006**, *27*, 2907–2915. [CrossRef] [PubMed]
36. Botor, M.; Fus-Kujawa, A.; Uroczynska, M.; Stepien, K.L.; Galicka, A.; Gawron, K.; Sieron, A.L. Osteogenesis Imperfecta: Current and Prospective Therapies. *Biomolecules* **2021**, *11*, 1493. [CrossRef] [PubMed]
37. van Tijum, R.; Vellinga, W.P.; De Hosso, J.; Th, M. Adhesion along metal–polymer interfaces during plastic deformation. *J. Mater. Sci.* **2007**, *42*, 3529–3536. [CrossRef] [PubMed]

38. Yamaguchi, S.; Le, P.T.M.; Shintani, S.A.; Takadama, H.; Ito, M.; Ferraris, S.; Spriano, S. Iodine-Loaded Calcium Titanate for Bone Repair with Sustainable Antibacterial Activity Prepared by Solution and Heat Treatment. *Nanomaterials* **2021**, *1*, 2199. [CrossRef] [PubMed]
39. Ferraris, S.; Yamaguchi, S.; Barbani, N.; Cazzola, M.; Cristallini, C.; Miola, M.; Vernè, E.; Spriano, S. Bioactive materials: In vitro investigation of different mechanisms of hydroxyapatite precipitation. *Acta Biomater.* **2019**, *102*, 468–480. [CrossRef]
40. Furuno, K.; Wang, J.; Suzuki, K.; Nakahata, M.; Sakai, S. Gelatin-Based Electrospun Fibers Insolubilized by Horseradish Peroxidase-Catalyzed Cross-Linking for Biomedical Applications. *ACS Omega* **2020**, *5*, 21254–21259. [CrossRef]
41. Dunford, J.E.; Thompson, K.; Coxon, F.P.; Luckman, S.P.; Hahn, F.M.; Poulter, C.D.; Ebetino, F.H.; Rogers, M.J. Structure-activity relationships for inhibition of farnesyl diphosphate synthase in vitro and inhibition of bone resorption in vivo by nitrogen-containing bisphosphonates. *J. Pharmacol. Exp. Ther.* **2001**, *296*, 235–242.